Ensemble-based simultaneous state and parameter estimation for treatment of mesoscale model error: A real-data study

Xiao-Ming Hu,[1] Fuqing Zhang,[1] and John W. Nielsen-Gammon[2]

Received 23 February 2010; revised 17 March 2010; accepted 25 March 2010; published 21 April 2010.

[1] This study explores the treatment of model error and uncertainties through simultaneous state and parameter estimation (SSPE) with an ensemble Kalman filter (EnKF) in the simulation of a 2006 air pollution event over the greater Houston area during the Second Texas Air Quality Study (TexAQS-II). Two parameters in the atmospheric boundary layer parameterization associated with large model sensitivities are combined with standard prognostic variables in an augmented state vector to be continuously updated through assimilation of wind profiler observations. It is found that forecasts of the atmosphere with EnKF/SSPE are markedly improved over experiments with no state and/or parameter estimation. More specifically, the EnKF/SSPE is shown to help alleviate a near-surface cold bias and to alter the momentum mixing in the boundary layer to produce more realistic wind profiles. **Citation:** Hu, X.-M., F. Zhang, and J. W. Nielsen-Gammon (2010), Ensemble-based simultaneous state and parameter estimation for treatment of mesoscale model error: A real-data study, *Geophys. Res. Lett.*, *37*, L08802, doi:10.1029/2010GL043017.

1. Introduction

[2] Accurate estimation of a system's state is intrinsically desirable and is critical for accurately forecasting its future states. The ensemble Kalman filter (EnKF), first proposed by *Evensen* [1994], has become increasingly popular for state estimation in geosciences (see recent review articles of *Evensen* [2003] and *Hamill* [2006]), including recent applications in air-pollution meteorology [e.g., *Stuart et al.*, 2007]. The primary advantage of the EnKF over traditional variational data assimilation methods is the use of flow-dependent error covariance derived from short-term ensemble forecasts along with its ease of implementation and seamless coupling with ensemble forecasting [*Zhang and Snyder*, 2007].

[3] Ideally, the ensemble of the first guesses would be drawn from the system attractor. However, because they are drawn from forecasts made by imperfect models, model error may cause all short-term forecasts to deviate from the system attractor, causing background error covariances to be estimated with respect to an incorrect state [*Hansen*, 2002]. Model error may be structural (model equations have a different functional form from the true laws governing the system) or parametric (the parameters used in model equations are not accurate). Structural model errors can often be converted into parametric errors by generalizing the functional forms [*Hansen*, 2002].

[4] The EnKF may account for model error through the state augmentation approach, by simultaneously estimating the optimal parameter values in addition to the conventional model state vector. Simultaneous state and parameter estimation with the EnKF has produced encouraging results when simulated observations from an independent simulation ("truth") are assimilated [*Annan et al.*, 2005a; *Hacker and Snyder*, 2005; *Aksoy et al.*, 2006a, 2006b; *Tong and Xue*, 2008]. This application of the EnKF not only may reduce the parametric errors directly, but may also offset structural errors to some extent [*Hansen and Penland*, 2007]. Thus simultaneous state and parameter estimation should help forecasts remain closer to the state attractor as they evolve and lead to better background-error covariance estimates, thereby improving subsequent analyses. Other, less direct ways of accounting for model error within the EnKF framework include covariance inflation/relaxation [*Zhang et al.*, 2004], and the use of multi-model multi-physics ensembles [*Meng and Zhang*, 2007].

[5] Few tests of the state augmentation approach have been performed with actual observations. When assimilating real data, simultaneous state and parameter estimation with the EnKF has also been shown to improve state estimation in climate modeling [*Annan et al.*, 2005b; *Kondrashov et al.*, 2008]. However, to the best of our knowledge, the effectiveness of the simultaneous state and parameter estimation with the EnKF in regional scale or mesoscale modeling applications has not been examined with real-data observations.

[6] In this study, the improvement of simultaneous state and parameter estimation over the regular state-estimation-only EnKF is investigated by estimating the values of certain fundamental parameters involving vertical mixing within the Weather Research and Forecast (WRF) model simultaneously with regular model state variables. Planetary boundary layer (PBL) schemes parameterize the turbulent vertical fluxes of heat, momentum and constituents such as moisture. Such schemes are important components of meteorological and air quality models. Errors and uncertainties associated with PBL schemes remain one of the primary sources of inaccuracies in model simulations [*Pleim*, 2007b]. Conventional PBL schemes are well-suited for parameter estimation because they include a variety of explicit or implicit parameters whose suboptimal specifications can cause observable systematic errors in model simulations.

[1] Department of Meteorology, Pennsylvania State University, University Park, Pennsylvania, USA.
[2] Department of Atmospheric Sciences, Texas A&M University, College Station, Texas, USA.

0094-8276/10/2010GL043017

[7] The scheme utilized here is the Asymmetrical Convective Model, version 2 (ACM2) PBL scheme [*Pleim*, 2007a, 2007b]. ACM2 includes an eddy diffusion component within the convective boundary layer in addition to the explicit nonlocal transport, and a weighting factor apportions the mixing due to local diffusion and nonlocal transport. Thus a common structural difference among PBL schemes is treated by ACM2 as a parameter. This makes the scheme particularly attractive for parameter estimation studies, although that particular parameter is not estimated here.

2. Methodology

2.1. Forecast Model: WRF

[8] The WRF model version 3.0.1 is used in this study [*Skamarock et al.*, 2005]. Three one-way nested domains are used with grid spacings of 108, 36, and 12 km, respectively. The coarse domain covers North and Central America, the second covers the contiguous United States and most of the Gulf of Mexico, the third covers Texas and adjacent portions of the southern United States. All model domains have 43 vertical layers, and the model top is set at 50 hPa. All model domains use Dudhia shortwave radiation, the rapid radiative transfer model (RRTM) for longwave radiation, the 6-class microphysics scheme (WSM6), the Noah land-surface scheme, the Grell-Dévényi ensemble convective parameterization, and the ACM2 PBL scheme with the Monin-Obukhov surface layer scheme. The National Centers for Environmental Prediction (NCEP) Global Forecast System (GFS) operational analyses and forecasts are used for all initial and boundary conditions except that the initial soil moisture is taken from the North American Regional Reanalysis (NARR). During the simulation period, the GFS has higher soil moisture over TX than other data sets (such as NARR) and earlier experiments showed that GFS soil moisture caused a significant cold bias over TX.

[9] Accurate representation of vertical mixing is particularly important in the simulation of transport and dispersion of pollutants, so an episode of poor air quality is selected. The simulations are conducted for the period from 1200 UTC August 29, 2006 to 0600 UTC September 2, 2006 over Texas. In the evening of August 29, there was a cold front passing Texas from north to south. In the wake of the frontal passage, northerly wind dominated at 850 hPa, which brought continental ozone and its precursors to Houston [*Rappenglück et al.*, 2008]. On August 31 and September 1, the poorest air quality indexes around Houston were recorded (http://www.tceq.state.tx.us/compliance/monitoring/air/monops/sigevents06.html).

2.2. Data Assimilation Method: EnKF

[10] The EnKF system used here is the same as that in the work of *Zhang et al.* [2009], except for the addition of parameter estimation. The parameter estimation version of the EnKF updates the augmented state vector (regular state variables plus parameters) simultaneously through the covariances sampled by the ensemble forecasts when new observations are assimilated. This EnKF uses the covariance relaxation of *Zhang et al.* [2004] to inflate the analysis error covariance at updated points via a weighted average between the prior perturbation (denoted by superscript f) and the posterior perturbation (denoted by superscript a) as follows:

$$(\mathbf{x}^a_{new})' = (1-\alpha)(\mathbf{x}^a)' + \alpha(\mathbf{x}^f)' \quad (1)$$

The weighting coefficient, α, is set to 0.8 as in the work of *Zhang et al.* [2009]. Unlike regular state variables whose ensemble spread usually increases during forecasting, the value of parameters in each ensemble member is kept constant during each forecast cycle. For regular state variables, covariance localization [*Gaspari and Cohn*, 1999] with radius of influence set to 30 grid points is performed in the full three-dimensional physical space. Unlike regular state variables, which are spatially variable, parameters to be estimated are assumed to be globally uniform in the WRF model. Contamination of the posterior estimate of the parameter may also occur through accumulation of sampling error during the update process if the number of observations is many orders of magnitude larger than the number of parameters to be estimated [*Aksoy et al.*, 2006a]. To avoid this, the "spatial updating" method of *Aksoy et al.* [2006a] was used here: first the parameters are updated horizontally as a two-dimensional array using localization, and then spatial averaging is performed to obtain global parameter values. Finally, the updated global parameter values are fed into the subsequent forecast cycle. A 30-member WRF ensemble is coupled with the EnKF for all analysis/forecasting cycles.

[11] In our parameter sensitivity experiments with ACM2 in WRF [*Nielsen-Gammon et al.*, 2010], two parameters controlling the vertical mixing in the PBL in particular show large and identifiable sensitivities, one for daytime (p, an exponent affecting the magnitude and vertical distribution of eddy diffusivity within the unstably stratified PBL) and one for nighttime (Rc, a critical Richardson number determining the transition between relatively large and small values of eddy diffusivity). Thus p and Rc are chosen to be the uncertain parameters to be estimated.

[12] The parameter p is shown to play the most important role in controlling the vertical distribution of heat and momentum during daytime [*Nielsen-Gammon et al.*, 2010]. In ACM2, p is taken to be 2. Among all parameters, Rc causes the largest variability of wind speed (>1 m s^{-1}) during nighttime around the level of nighttime low-level jet [*Nielsen-Gammon et al.*, 2010]. In ACM2, Rc is taken to be 0.25. The realistic ranges of parameter values are inferred to be $1 < p < 3$ and $0.1 < \mathrm{Rc} < 1.0$ by *Nielsen-Gammon et al.* [2010]. In order to constrain the model parameters to lie within their physically realistic ranges, a parameter transformation technique [*Nielsen-Gammon et al.*, 2010] is used to transform any model parameter x to a normal parameter y by

$$x = A + \left(0.5 + \frac{\arctan(y)}{\pi}\right)(B - A) \quad (2)$$

With this formulation, y varies from +/− infinity while x varies within the range [*A:B*]. Parameter estimation is performed on y, and y is transformed to x prior to its use in ACM2 for WRF model integrations.

[13] In the initial ensemble forecasting period (1200 UTC August 29-0000 UTC August 30), two sets of 30 pseudo-random values drawn from a normal distribution with zero mean and a standard deviation of 1.0 are generated for p and

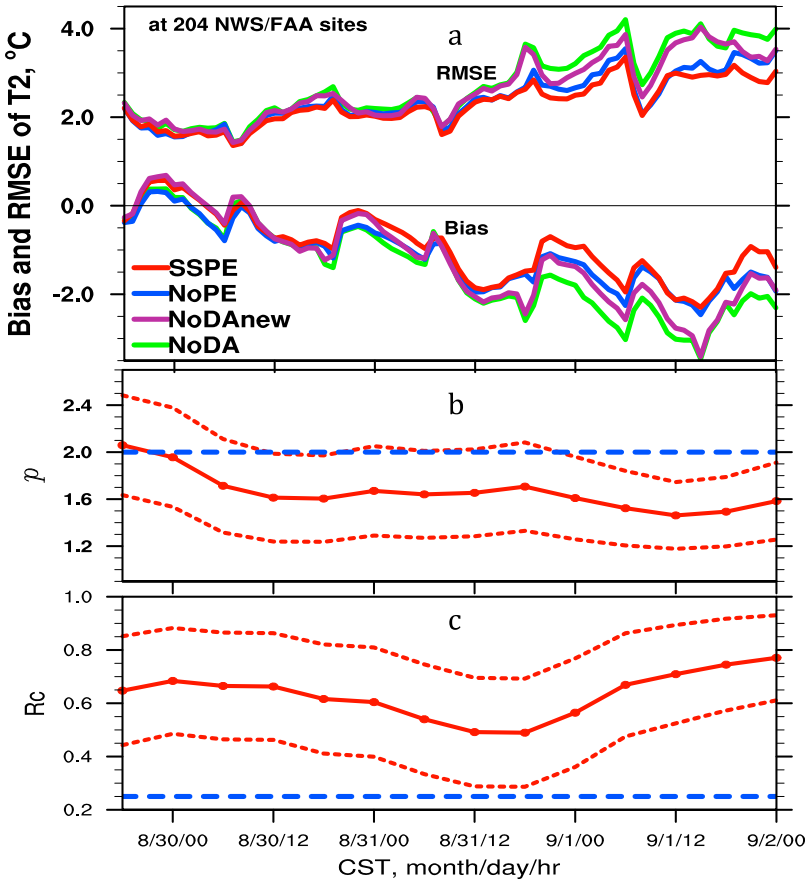

Figure 1. Mean bias of 2 m temperature over (a) NWS/FAA sites from NoDA (deterministic forecasting), NoPE (EnKF but no PE), SSPE (simultaneous state and parameter estimation with EnKF), NoDAnew (deterministic forecasting with estimated p and Ri from SSPE) and estimated (b) p and (c) Rc by SSPE. The dashed lines in Figures 1b and 1c show the standard deviation of parameter spread and a straight dashed line is drawn at the default values of p and Rc.

Rc. The 30 pseudo-random values are then transformed to the specific range of each parameter using (2). A different transformed set of parameter values is used in each member of the WRF ensemble. The parameter values are updated simultaneously with state variables when new observations are assimilated.

[14] Since these two PBL parameters primarily control mixing in the PBL, assimilated observational data that include information regarding the vertical distribution of state variables are particularly valuable [*Nielsen-Gammon et al.*, 2010]. Here, radar wind profiler data from the TexAQS-II network [*Parrish et al.*, 2009] are assimilated starting from 0000 UTC 30 August through 0600 UTC 2 September every six hours. Most profiler data are from 915 MHz profilers except for three tropospheric profilers at Jayton (JTN), Ledbetter (LDB), and Palestine (PAT) that provide relatively coarse data up to 16 km. Radar wind profilers operating at 915 MHz provide high-density wind data in the PBL and the lower free troposphere.

[15] Four experiments are conducted, which include (1) a deterministic WRF forecast without data assimilation ("NoDA"), (2) assimilation of profiler observations with the EnKF but without parameter estimation ("NoPE"), (3) simultaneous state and parameter estimation with the EnKF using the parameter transformation technique ("SSPE"), and (4) a deterministic WRF forecasting as in NoDA but with updated values of p and Ri estimated from SSPE ("NoDAnew"). Model output intercomparisons and diagnoses are carried out on the innermost (12 km) domain. Validation is performed against the dependent radar wind profiler data set and against independent surface observations of wind and temperature.

3. Results

[16] Figure 1a shows the time evolution of the mean bias and root mean square error (RMSE) of the 2-m temperature (T2) with respect to the unassimilated hourly observations at the 204 National Weather Service and Federal Aviation Administration (NWS/FAA) sites simulated by the ensemble means in experiments NoDA, NoPE, SSPE, and NoDAnew. At the beginning of all simulations, the bias and RMSE of simulated T2 are relatively small. A cold bias appears during the following day and increases on subsequent days. Among all experiments, NoDA shows the largest cold bias and cold drift. NoPE shows significant improvement over NoDA in terms of both bias and RMSE, which means assimilating wind profiler data benefited temperature prediction substantially. The SSPE experiment achieved the smallest cold bias and RMSE of all experiments. NoDAnew performed worse than NoPE and SSPE but better than NoDA. Differences in performance between SSPE and NoPE clearly show the benefit of parameter estimation beyond state estimation with the EnKF.

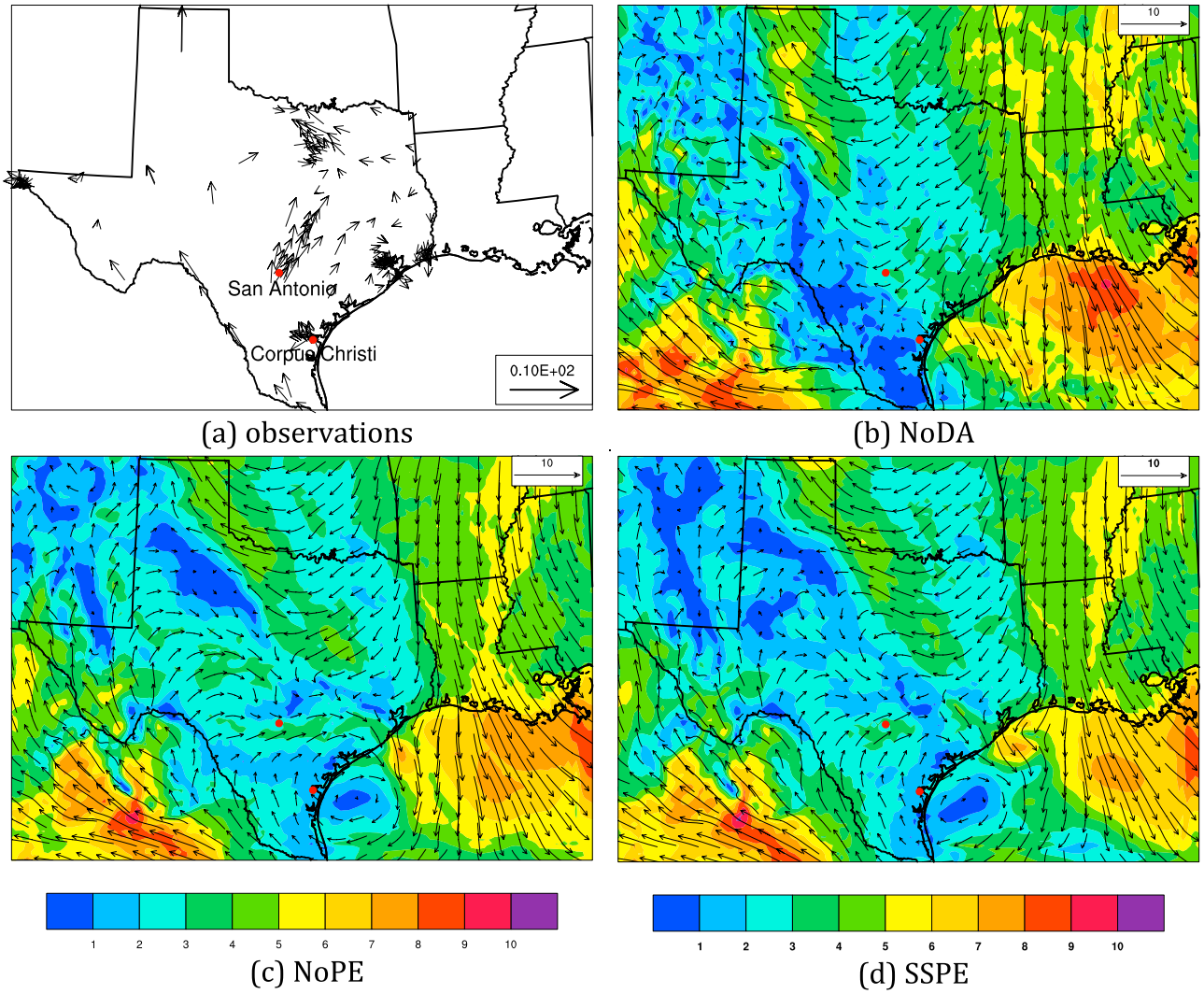

Figure 2. Wind vectors at September 1, 10 CST at 10 m AGL from (a) observations, (b) NoDA (deterministic forecast), (c) NoPE (EnKF but no PE), and (d) SSPE (simultaneous state and parameter estimation with EnKF). The shaded color is the magnitude of wind speed.

[17] The time evolution of the two uncertain parameters (p and Rc) estimated by experiment SSPE is shown in Figures 1b–1c. SSPE estimated p to be lower than its default value 2.0 throughout the experiment except for 18 CST 29 August and estimated Rc to be always higher than its default value of 0.25. The ensemble parameter spread decreases throughout the period, but slowly enough that the spread still spans a large portion of the expected uncertainty.

[18] The ending values of p and Rc from SSPE were 1.59 and 0.77, respectively. The change in p has the consequence of causing a 33% increase in the local mixing coefficient at the midpoint of the convective boundary layer, with larger increases near its top. The change in Rc permits much more vigorous mixing under stable stratification near the shear instability threshold, but has no direct effect on the vertical mixing coefficient beyond Ri = 0.77.

[19] In NoDAnew, the parameters p and Rc were updated every 6 hours using the estimated values from SSPE during the preceding 6-hour analysis cycle (as in SSPE). NoDAnew consistently outperformed NoDA (Figure 1a) and at times achieved reductions of bias and RMSE similar to that achieved through standard EnKF data assimilation (NoPE). This forecast improvement, purely from the use of new fixed parameter values, suggests the promising possibility of using the EnKF and state observations to tune parameter values to obtain better-performing physics parameterizations. Given the slow changes of both parameter values from one analysis cycle to the next (Figure 1b), we speculate similar performance would be obtained if we updated the parameter values with the SSPE estimation from the same analysis cycle.

[20] A cold drift in deterministic WRF forecasts of this period (with a different boundary-layer scheme) is also reported by *Wilczak et al.* [2009] for simulations over Texas, accompanied by too strong northerly winds and/or too weak southerly winds. During our simulation period, the dominant large scale flow over Texas is a northerly wind, with a northerly jet present immediately above the PBL over eastern Texas. The cold drift of our simulations may be partially caused by the simulated too strong northerly wind, producing too much cold advection. An example of errors in the simulated winds is shown in Figure 2. In Figure 2b, the deterministic forecast predicts that northerly winds should

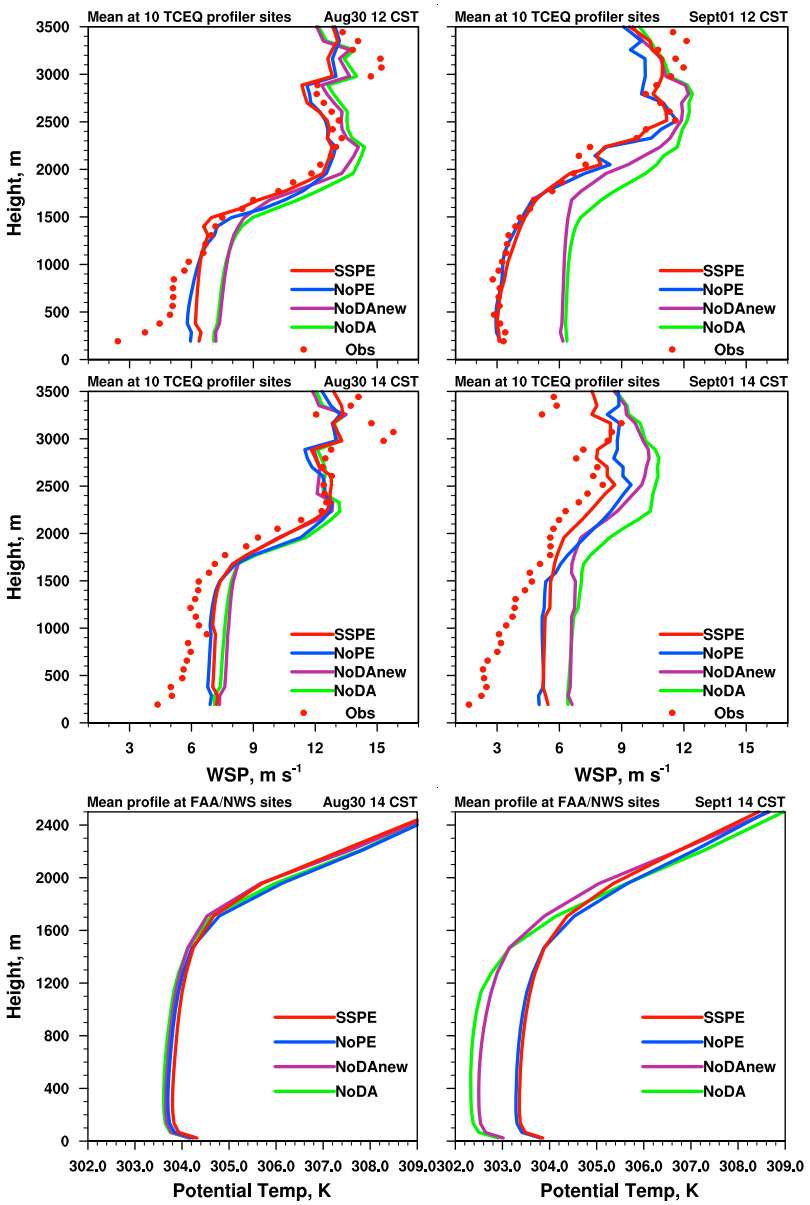

Figure 3. Mean wind speed profile over 10 central and eastern Texas profiler sites at 12, 14 CST (row 1–2) and mean temperature profile over NWS/FAA sites at 14 CST (row 3), August 30 and September 1 from observations (Obs) and model experiments NoDA (deterministic forecast), NoPE (EnKF but no PE), SSPE (simultaneous state and parameter estimation with EnKF), and NoDAnew (deterministic forecast with estimated p and Ri from SSPE).

dominate over eastern Texas at 10 CST, September 1. However, according to the independent observations shown in Figure 2a, some local sea breezes have developed along the southern Texas coast. The winds near Corpus Christi are mainly easterly/southeasterly and the wind near San Antonio is southerly or southwesterly. As seen in Figure 1, the EnKF assimilation without parameter estimation (NoPE) did reduce the cold bias to some extent, apparently from improved boundary-layer wind representation. For example, the NoPE run produces a wind pattern over southern Texas (Figure 2c) that is somewhat similar to what was observed (Figure 2a), although substantial differences still exist (e.g., the observed wind at San Antonio is southerly while the wind simulated by NoPE is westerly).

[21] A cold bias can also be caused directly by a simulated PBL that is too shallow. Indirectly, a shallow PBL may cause an underestimation of the magnitude of surface drag, thereby causing the prevailing boundary-layer northerly winds to be too strong. Parameter sensitivity tests on ACM2 conducted by *Hu et al.* [2010] showed that the daytime PBL height is sensitive to the value of the parameter p. Other tests have shown that wind speed has large covariance with p and has the largest sensitivity to p near the top of the PBL [*Nielsen-Gammon et al.*, 2010]. A large difference between the first-guess and observed wind near the top of the daytime PBL would therefore cause a large increment of p in SSPE, thereby altering the daytime PBL depth and temperatures within the PBL.

[22] Figure 3 shows the mean wind speed profiles at 12 and 14 CST on both August 30 and September 1 over the 10 profilers sites that have the most complete observations (Brenham (BHM), Beeville (BVL), Cleburne (CLE),

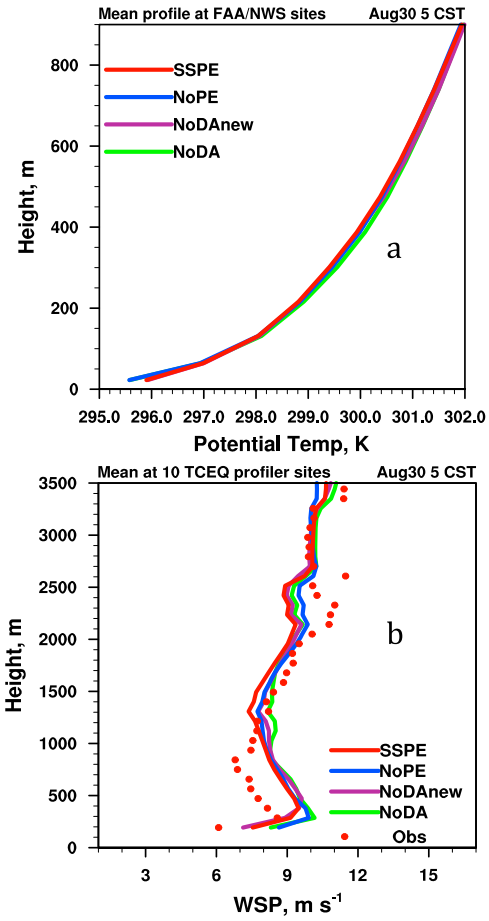

Figure 4. (a) Mean profiles of potential temperature at 5 CST, August 30 over NWS/FAA sites from model experiments and (b) mean wind speed profiles at the same time over profiler sites from observations and model experiments.

Huntsville (HVE), Jefferson County (JEF), Ledbetter (LDB), LaPorte (LPT), Longview (LVW), Moody (MDY), and Palestine (PAT)) in comparison with estimations from experiments NoDA, NoPE, SSPE and NoDAnew. In the EnKF runs NoPE and SSPE, data assimilation takes place at 12 CST and the 14 CST output represents a 2-h forecast. A wind maximum is apparent on both days at about 2500–3000 m (as well as August 31, not shown). Below the jet, a layer of near-uniform wind speed, signifying the daytime mixed layer, is present up to 1500–1800 m. The deterministic forecast NoDA overpredicts wind speed substantially in the PBL on all three days. Experiment NoPE, with state estimation only, has much-improved wind speeds in the PBL, but the wind speeds at the top of and above the PBL are still overpredicted.

[23] Since smaller p leads to stronger mixing and lower wind speeds near the top of PBL [*Hu et al.*, 2010; *Nielsen-Gammon et al.*, 2010], SSPE should cause the estimated value of p to decrease. Indeed, p is estimated to be lower than its default value of 2.0 except for 18 CST, August 29, and the lowest values (~1.5–1.6) in SSPE occur while daytime observations are assimilated (Figure 1). With lower values of p, a deeper PBL and a higher and weaker jet above the PBL are simulated by SSPE (Figure 3). Since the large-scale northerly flow is reduced and the wind maximum is farther above the ground, local-scale circulations can develop more easily. SSPE produces surface winds with patterns that agree best with independent observations, with a southeasterly wind at Corpus Christi and a southwesterly wind at San Antonio (Figure 2d). In NoDAnew, using the SSPE-estimated p and Rc values, a deeper PBL and a higher and weaker jet above the PBL are simulated (Figure 3) and consequently the southerly wind in southern TX is more prominent (not shown). Since SSPE predicts a deeper PBL, air is entrained from higher altitudes, warming the PBL as seen in the temperature profile in the bottom row of Figure 3. This effect combines with the reduced transport of cooler air from the north to reduce the cold bias at the surface (Figure 1a).

[24] The wind speed in the lower troposphere predicted by NoDA is also too strong at night (Figure 4). NoPE produces a small but systematic improvement, while SSPE again produces the best agreement with observations below 1000m. Larger values of Rc (>0.5, compared to the default value of 0.25) are estimated during nighttime by SSPE as seen in Figure 1, increasing the vertical mixing and reducing the nighttime low level jet (LLJ). Consequently the larger Rc causes stronger nighttime mixing and increased surface temperatures (Figure 4a), thereby reducing the model's cold bias (Figure 1). Thus SSPE gives the best performance for both wind and temperature during both daytime and nighttime at most levels and times. The use of SSPE-estimated parameters in NoDAnew leads to less bias in predictions of nighttime winds and temperatures (Figures 1 and 4) than NoDA.

4. Conclusions and Discussion

[25] The EnKF is used here to estimate the flow-dependent optimal values of two parameters fundamental to the performance of the ACM2 PBL scheme in the WRF model through the state vector augmentation method. Simulations are conducted for the period 1200 UTC August 29, 2006 to 0600 UTC September 2, 2006 over Texas using WRF deterministic forecasts, conventional EnKF, EnKF with parameter estimation, and WRF deterministic forecasts with estimated parameters. The EnKF simulations assimilate radar wind profiler observations every six hours. A cold drift is found in the WRF deterministic forecasts that is suspected to be partly caused by northerly winds simulated to be too strong and a daytime PBL simulated to be too shallow. Conventional EnKF improves the wind fields somewhat and produces an improvement in temperatures. Parameter-estimation EnKF results in a much greater reduction in the model biases of both wind and temperature. Also, pure forecasts with updated parameters outperform forecasts with standard parameter settings.

[26] Despite the improvement, some biases remain. It is possible that the underlying cause of the model error is not the PBL scheme at all but rather some other simulated physical process, in which case parameter estimation is producing the right answer for the wrong reasons. One such source of error that may be masked by adjustments to the PBL scheme are errors in land surface characteristics, such as moisture availability. Application of parameter estimation to include other empirical or uncertain parameters in the PBL and/or other physics parameterization schemes may produce additional improvement. It is also possible that the

absence of strong chaotic dynamics in the PBL in some circumstances may adversely affect the EnKF/SSPE performance [e.g., *Hacker and Snyder*, 2005]. Nevertheless, with the configuration of WRF employed here and this particular simulated episode, parameter estimation produces better analyses and more realistic simulations when measured against both dependent and independent data. Ongoing and future research will examine the consistency and effectiveness of parameter estimations for other events, including the additional estimation of other uncertain parameters in the forecast model.

[27] **Acknowledgments.** This work was supported by the State of Texas through a contract from the Houston Advanced Research Center, the Texas Environmental Research Consortium, the Texas Commission on Environmental Quality, and the National Science Foundation grant ATM-0840651. Yonghui Weng assisted us with implementation of the parameter estimation EnKF.

References

Aksoy, A., F. Zhang, and J. W. Nielsen-Gammon (2006a), Ensemble-based simultaneous state and parameter estimation with MM5, *Geophys. Res. Lett.*, *33*, L12801, doi:10.1029/2006GL026186.

Aksoy, A., F. Zhang, and J. W. Nielsen-Gammon (2006b), Ensemble-based simultaneous state and parameter estimation in a two-dimensional sea-breeze model, *Mon. Weather Rev.*, *134*, 2951–2970, doi:10.1175/MWR3224.1.

Annan, J. D., J. C. Hargreaves, N. R. Edwards, and R. Marsh (2005a), Parameter estimation in an intermediate complexity earth system model using an ensemble Kalman filter, *Ocean Modell.*, *8*, 135–154, doi:10.1016/j.ocemod.2003.12.004.

Annan, J. D., J. D. Lunt, J. C. Hargreaces, and P. J. Valdes (2005b), Parameter estimation in an atmospheric GCM using the ensemble Kalman filter, *Nonlinear Processes Geophys.*, *12*, 363–371.

Evensen, G. (1994), Sequential data assimilation with a nonlinear quasi-geostrophic model using Monte Carlo methods to forecast error statistics, *J. Geophys. Res.*, *99*, 10,143–10,162, doi:10.1029/94JC00572.

Evensen, G. (2003), The ensemble Kalman filter: Theoretical formulation and practical implementation, *Ocean Dyn.*, *53*, 343–367, doi:10.1007/s10236-003-0036-9.

Gaspari, G., and S. E. Cohn (1999), Construction of correlation functions in two and three dimensions, *Q. J. R. Meteorol. Soc.*, *125*, 723–757, doi:10.1002/qj.49712555417.

Hacker, J. P., and C. Snyder (2005), Ensemble Kalman filter assimilation of fixed screen-height observations in a parameterized PBL, *Mon. Weather Rev.*, *133*, 3260–3275, doi:10.1175/MWR3022.1.

Hamill, T. M. (2006), Ensemble-based atmospheric data assimilation, in *Predictability of Weather and Climate*, edited by T. Palmer and R. Hagedorn, chap. 6, pp. 124–156, Cambridge Univ. Press, Cambridge, U. K.

Hansen, J. A. (2002), Accounting for model error in ensemble-based state estimation and forecasting, *Mon. Weather Rev.*, *130*, 2373–2391, doi:10.1175/1520-0493(2002)130<2373:AFMEIE>2.0.CO;2.

Hansen, J., and C. Penland (2007), On stochastic parameter estimation using data assimilation, *Physica D*, *230*, 88–98, doi:10.1016/j.physd.2006.11.006.

Hu, X.-M., J. W. Nielsen-Gammon, and F. Zhang (2010), Evaluation of three planetary boundary layer schemes in the WRF model, *J. Appl. Meteorol. Climatol.*, in press.

Kondrashov, D., C.-J. Sun, and M. Ghil (2008), Data assimilation for a coupled ocean-atmosphere model. Part II: Parameter estimation, *Mon. Weather Rev.*, *136*, 5062–5076, doi:10.1175/2008MWR2544.1.

Meng, Z., and F. Zhang (2007), Test of an ensemble Kalman filter for mesoscale and regional-scale data assimilation. Part II: Imperfect model experiments, *Mon. Weather Rev.*, *135*, 1403–1423, doi:10.1175/MWR3352.1.

Nielsen-Gammon, J. W., X.-M. Hu, F. Zhang, and J. E. Pleim (2010), Evaluation of planetary boundary layer scheme sensitivities for the purpose of parameter estimation, *Mon. Weather Rev.*, in press.

Parrish, D. D., et al. (2009), Overview of the Second Texas Air Quality Study (TexAQS II) and the Gulf of Mexico Atmospheric Composition and Climate Study (GoMaACCS), *J. Geophys. Res.*, *114*, D00F13, doi:10.1029/2009JD011842.

Pleim, J. E. (2007a), A combined local and nonlocal closure model for the atmospheric boundary layer. Part I: Model description and testing, *J. Appl. Meteorol. Climatol.*, *46*, 1383–1395, doi:10.1175/JAM2539.1.

Pleim, J. E. (2007b), A combined local and nonlocal closure model for the atmospheric boundary layer. Part II: Application and evaluation in a mesoscale meteorological model, *J. Appl. Meteorol. Climatol.*, *46*, 1396–1409, doi:10.1175/JAM2534.1.

Rappenglück, B., R. Perna, S. Zhong, and G. A. Morris (2008), An analysis of the vertical structure of the atmosphere and the upper-level meteorology and their impact on surface ozone levels in Houston, Texas, *J. Geophys. Res.*, *113*, D17315, doi:10.1029/2007JD009745.

Skamarock, W. C., J. B. Klemp, J. Dudhia, D. O. Gill, D. M. Barker, W. Wang, and J. G. Powers (2005), A description of the advanced research WRF version 2, *Tech. Note NCAR/TN-468+STR*, Natl. Cent. for Atmos. Res., Boulder, Colo.

Stuart, A. L., A. Aksoy, F. Zhang, and J. W. Nielsen-Gammon (2007), Ensemble-based data assimilation and targeted observation of a chemical tracer in a sea breeze model, *Atmos. Environ.*, *41*, 3082–3094, doi:10.1016/j.atmosenv.2006.11.046.

Tong, M., and M. Xue (2008), Simultaneous estimation of microphysical parameters and atmospheric state with simulated radar data and ensemble square root Kalman filter. Part II: Parameter estimation experiments, *Mon. Weather Rev.*, *136*, 1649–1668, doi:10.1175/2007MWR2071.1.

Wilczak, J. M., I. Djalalova, S. McKeen, L. Bianco, J.-W. Bao, G. Grell, S. Peckham, R. Mathur, J. McQueen, and P. Lee (2009), Analysis of regional meteorology and surface ozone during the TexAQS II field program and an evaluation of the NMM-CMAQ and WRF-Chem air quality models, *J. Geophys. Res.*, *114*, D00F14, doi:10.1029/2008JD011675.

Zhang, F., and C. Snyder (2007), Ensemble-based data assimilation, *Bull. Am. Meteorol. Soc.*, *88*, 565–568, doi:10.1175/BAMS-88-4-565.

Zhang, F., C. Snyder, and J. Sun (2004), Tests of an ensemble Kalman filter for convective-scale data assimilation: Impact of initial estimate and observations, *Mon. Weather Rev.*, *132*, 1238–1253, doi:10.1175/1520-0493(2004)132<1238:IOIEAO>2.0.CO;2.

Zhang, F., Y. Weng, J. A. Sippel, Z. Meng, and C. H. Bishop (2009), Cloud-resolving hurricane initialization and prediction through assimilation of Doppler radar observations with an ensemble Kalman filter: Humberto (2007), *Mon. Weather Rev.*, *137*, 2105–2125, doi:10.1175/2009MWR2645.1.

X.-M. Hu and F. Zhang, Department of Meteorology, Pennsylvania State University, University Park, PA 16802, USA.

J. W. Nielsen-Gammon, Department of Atmospheric Sciences, Texas A&M University, College Station, TX 77843, USA.